Evaluation of Microstructure and Fracture Characteristics Based on Cooling Rates of SA508 Gr.1A Low-Alloy Steel

Se-Mi Hyun[a], Seokmin Hong[a], Jongmin Kim[a], Min-Chul Kim*[a]

[a]*Materials Safety Technology Research Division, Korea Atomic Energy Research Institute, Deokjin dong, Daejeon, Korea*
[*]*Corresponding author: mckim@kaeri.re.k*

Keywords : SA508 Gr.1A Low-Alloy Steel, Phase Fraction, Fracture Toughness, Cooling Rate

1. Introduction

The main steam line (MSL) piping in nuclear power plants (NPPs) is manufactured through austenitization heat treatment followed by water quenching and tempering processes [1]. The cooling rate varies depending on the thickness of the pipes, leading to differences in microstructure [2]. Microstructural features such as phase fraction, grain size, and precipitate size generally influenced the mechanical properties of the materials [3]. Therefore, studying the effects of cooling rate on microstructure formation and changes in mechanical properties is essential to achieve the desired mechanical properties. Previous studies have primarily focused on materials with distinct microstructural characteristics, but there has been a lack of research on how the phase fraction in low-alloy steels with two or more phases affects mechanical properties.

In this study, dilatometry analysis was used to confirm the phase transformation behavior of low-alloy steel at cooling rates of 0.3°C/s, 1.2°C/s, and 15°C/s, corresponding to the cooling rates of actual heat-treated blocks. Additionally, the effect of changes in phase fraction due to cooling rate on fracture properties was analyzed.

2. Methods and Results

2.1 Materials and heat treatment

In this study, SA508 Gr.1a low-alloy steel, manufactured by adjusting the content of Mo and V to improve strength, was used. To analyze the phase fractions and fracture characteristics based on cooling rates, the small blocks (130 mm (L) ×150 mm (W) ×38mm (T)) were austenitized at 880 °C for 2 hours and then subjected to various cooling methods, including water quenching (WQ), air quenching (AQ), air cooling (AC), and furnace cooling (FC). The blocks were named based on their cooling rate conditions: the block cooled by FC was labeled as "F," AC as "A," AQ as "Q," and WQ as "W.

2.2 Dilatometry Analysis

To analyze the phase transformation behavior at different cooling rates, specimens with a diameter of 4 mm and a length of 10 mm were used. Dilatometry analysis was conducted using the DIL 805L equipment (Theta Industries, USA) under cooling conditions of 0.3°C/s, 1.2°C/s, and 15°C/s, matching the cooling rates of the actual heat-treated blocks.

Dilatometry analysis revealed that under the conditions of 0.3°C/s and 1.2°C/s, a mixed microstructure of ferrite, pearlite, and bainite was formed. In contrast, at the rapid cooling condition of 15°C/s, most of the microstructure consisted of low-temperature transformation phases, specifically bainite and martensite.

2.3 Microstructure

The longitudinal - transverse (L-T) surfaces were polished and etched with 3% nital solution to analysis the microstructures of each heat-treated sample, using an optical microscope (OM; Nikon Eclipse-MA200, Japan) and a thermal field-emission scanning electron microscope (FE-SEM; Thermo Scientific Scios 2, USA).

The fraction of high-temperature microstructure such as ferrite and pearlite decreased, while the fraction of low-temperature transformation microstructure increased. F was mainly composed of ferrite (72%) and pearlite (28%), whereas A showed a decreased fraction of ferrite and pearlite with a small amount of bainite. Compared to A, Q had an increase in the fraction of bainite from 9% to 38%, and W formed the finest low-temperature transformation microstructure.

2.4 Mechanical testing

Tensile tests were conducted using round tensile specimens (gauge length of 25 mm, diameter of 6.25 mm) prepared in the transverse (T) direction in accordance with the ASTM A370 standard [4]. The tests were performed at 286 °C with a strain rate of 5.2×10^{-4} /s using an MTS universal testing machine (MTS 810.24, MTS Systems Corporation, USA). The tensile properties, including yield strength, tensile strength, and total elongation, were obtained from the stress-strain curves, with the yield strength determined by the 0.2% offset method. The engineering stress-strain curve at 286°C is shown in Fig. 1. As the cooling rate increased, both yield strength and tensile strength improved. Additionally, as the cooling rate increased, serration, indicative of dynamic strain aging, appeared, becoming especially pronounced in specimen W. As a result, the yield strength and tensile strength of

specimen W were approximately 250 MPa and 150 MPa higher, respectively, than those of specimen F, showing a significantly greater increase compared to the other specimens.

Charpy ductile-brittle transition test was conducted in according with ASTM E23 [5], using the impact tester machine (model : DTI-603D) with a capacity of 500 J. Charpy V-notch specimens (10 mm × 10 mm × 55 mm) in the transverse–longitudinal (T-L) direction, within a temperature range of –100 to 50 °C. Charpy ductile-brittle transition curves were obtained using the hyperbolic tangent curve-fitting method based on temperature-dependent absorbed energies [6]. From the curves, the upper shelf energy (USE), index temperatures (T_{41J}, T_{68J}), and the ductile-brittle transition temperature (DBTT) were determined. The T_{41J} and T_{68J} notations refer to the temperatures at which the absorbed energy is 41 J and 68 J, respectively, and are used to evaluate the transition characteristics. The Charpy ductile-brittle transition curve for each material at different temperatures is shown in Fig. 2. As the cooling rate increased, the USE tended to increase for all specimens except A. The T_{41J} and T_{68J} values were similar for F and A, and it was observed that the transition temperature decreased as the cooling rate increased. Notably, W, with the fastest cooling rate, exhibited the lowest T_{41J}, T_{68J}, and DBTT, indicating the greatest improvement in impact transition characteristics.

J-R fracture resistance test was conducted using a compact tension (1T-CT) specimen in accordance with ASTM E1820 [7]. The test was performed at the operating temperature of the MSL piping, 286 °C, with a testing speed of 0.5 mm/min. A fatigue pre-crack was generated at room temperature. The J-R curve for each specimen was obtained from the load-displacement data. In accordance with ASTM E1820 [7], the J_{Ic} values satisfied the validity criteria and were evaluated accordingly. As the cooling rate increased from F to A, the fraction of coarse pearlite decreased, leading to an improvement in J-R fracture resistance. However, in Q and W, the J_{Ic} values decreased due to the increase in the fraction of fine low-temperature transformation phases, which induced localized deformation through DSA. Particularly, in W, where DSA was more pronounced, the J_{Ic} value was the lowest at 539 kJ/m².

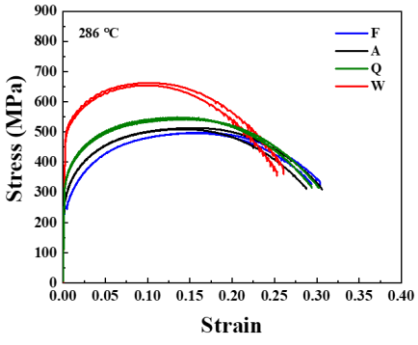

Fig. 1. Engineering stress-strain curves

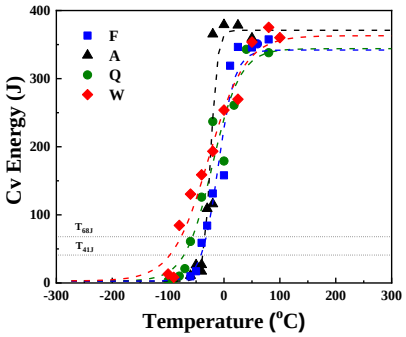

Fig. 2. Charpy ductile-brittle transition curve

3. Conclusions

1. As the cooling rate increased, the fraction of low-temperature transformation microstructures increased, significantly enhancing the tensile properties at 286 °C.
2. The formation of fine low-temperature transformation microstructure led to a reduction in grain and precipitate size, resulting in an improvement in impact transition characteristics. Notably, in W, the T_{41J} and DBTT values were the lowest, indicating a significant enhancement in fracture toughness.
3. DSA became more pronounced with the increase in the formation of low-temperature transformation microstructures, particularly in W. As a result, despite the tensile properties showing the greatest improvement, the J-R fracture resistance value was the lowest at 539 kJ/m².

REFERENCES

[1] ASTM Standard A508/A508M-16, ASTM Int., 2016.
[2] S.M, Hong, K.D. Min, S.M. Hyun, J.M. Kim, Y.S. Lee, H.D. Kim, M.C. Kim, Int. J. Press. Vessel. Pip., 191, pp.104359, 2021.
[3] S.M. Hyun, S. Hong, M.C. Kim, J.M. Kim, S.S. Sohn, S.I. Hong, Mater. Sci. Eng. A., 811, pp.1411069, 2021
[4] ASTM Standard A370-24, ASTM Int., 2024.
[5] ASTM Standard E23-24, ASTM Int., 2024.
[6] W. Oldfield, ASTM Standardization News 3, 24 1975.
[7] ASTM Standard E1820-23b, ASTM Int., 2023.